ATLASES OF ORIENTABILITY FOR ROBOTIC MANIPULATOR ARMS

Karim Abdel-Malek
Department of Mechanical Engineering
American University of Beirut NY Office
850 Third Avenue
New York, NY 10022

Harn-Jou Yeh
Center for Computer Aided Design
Department of Mechanical Engineering
The University of Iowa
Iowa City, IA 52242

Abstract

Maps illustrating all possible orientations of a manipulator are presented. These maps are called atlases of orientability. The formulation is intended to improve the understanding of the functionality of manipulators used in robot-assisted surgery. A surgeon, for example, may use these tools in order to obtain an understanding of the manipulability of the robot and to better locate the target. The problem for a general open kinematic chain manipulator is formulated using the Denavit-Hartenberg representation. A manipulator is segmented into two parts. A point, called the wrist point, is identified such that its workspace is determined (wrist workspace). Analytical boundary of the wrist workspace is formulated. Distal links beyond the wrist point are also studied to determine the boundary of their workspace. The two sets of boundaries are then intersected, and intersection curves are projected on a two-dimensional space to display atlases of orientability. Difficulties encountered in tracing curves, determining singularities of the Jacobian, and plotting the boundary of the workspace are discussed. The formulation is illustrated by implementing it to a planar three-degree-of-freedom manipulator and a spatial six-degree-of-freedom manipulator.

Key Words Manipulators, Kinematics, workspace, Dexterity

1. Introduction

In this paper, maps that illustrate orientability of the end-effector of a manipulator are analytically developed and are called atlases of orientability. Before addressing this problem, it is advantageous to set an application area where this analytic method can be used. A surgeon, for example, may use these charts to (1) determine all orientations of a manipulator at a target and (2) identify a location for the manipulator such that optimum orientability is achieved.

The tools developed in this paper are used in a robot-assisted surgery procedure. Robots have been used in the manufacturing industry to increase the productivity and accuracy of many functions such as welding cars, manufacturing metal and plastic products, assembling electronic components, palletizing cartons, and loading and unloading machines. Robots, however, have not made a significant impact on the health care system. Although the implementation of manipulator arms into surgical procedures has met with some success and is seen to have great potential, only a few researchers have addressed the needs of the medical industry to specific tools in the robotics field.

There are many areas in robot-assisted surgery that require further study and development. Issues such as fixation methods of the target with respect to the manipulator arm need to be studied. Knowledge of the absolute coordinates of the target (called registration) with respect to the reference frame is also one of the difficulties that has not been resolved. Locating the manipulator arm in such a manner to obtain maximum functionality with respect to the target is one of these difficulties that is addressed in this paper.

Robots have been used in surgery to guide tools on the basis of a digitized imagery such as Computed Tomography (CT) or Magnetic Resonance Imaging (MRI) of a fixed patient. These manipulator arms are used to remove tumors, abscesses, and hematomas. A manipulator called SARAH (Surgeon Assistant Robot Acting on the Head), for example, has been successful in

carrying out tumor resection as well as microdrilling in stapedectomy and laser ablation of deep-seated neck tumors [1]. The manipulator was used in order to obtain several orientations of the resection needle attached to the end-effector. A Unimation PUMA 200 robot was used by Kwoh [2] in conjunction with a CT scanner to resect brain tumors that needed to be approached through different directions. In the system reported by Benabid et al. [3] and Lavallee and Cinquin [4], a manipulator using two X-ray photos, accesses the center of the skull by choosing the best orientation.

This paper aims to develop a tool to aid in locating the manipulator with respect to a target in order to obtain optimum orientability. Atlases of orientability of a manipulator at a target are introduced. First, manipulator kinematics are studied to determine the positioning system of a chosen point called the wrist point. This system is studied to determine singular surfaces at which the manipulator loses at least one degree of mobility. Atlases of orientability at a known point in the workspace of the manipulator are developed by studying the penetration of the end-effector to an imaginary sphere (called the service sphere) built around the target. Points of penetration are determined by computing the intersection of this sphere with the surfaces enveloping the wrist workspace. To clarify terms used throughout this discussion, a definition of terms follows.

Atlases of Orientability: Maps that depict all possible orientations at a point in the workspace.

Singular Surface: A surface in the workspace upon which the manipulator loses at least one degree of mobility such that the wrist point can move only on this surface.

Singular Curve: A curve that results from the intersection of two singular surfaces such that the manipulator loses at least two degrees of mobility (the wrist point moves along a curve).

Service Sphere: A sphere located at a specified point in the workspace used to depict all possible penetrations of the end effector. This sphere is used as a measure of orientability.

Service Regions: Regions on the service sphere where penetration of the end-effector occurs.

Distal Links: Links of the manipulator that are located beyond the wrist point.

Wrist Workspace: The volume in space that contains all points attained by the wrist point.

In this paper, first-order singularities of the position-mechanism are computed using the determinant of the Jacobian. Second-order singularities are not computed directly. However, singular curves representing second-order singularities are traced numerically. These curves are then projected onto a parametric space. The paper also addresses difficulties in determining the intersection between singular curves.

There has been numerous works in the field of workspace and singularity analysis of robotic manipulators. A numerical approach to determining the workspace was formulated and solved by Kumar and Waldron [5] by tracing boundary surfaces of a workspace. Tsai and Soni [6] studied accessible regions of planar manipulators, while Gupta and Roth [7] studied the effect of hand size on workspace analysis. Recently, Haug et al. [8] formulated numerical criteria to find the workspace (so-called accessible output set) of a general multi-degree-of-freedom system via the study of a row-rank deficiency of its Jacobian. The algorithm computes tangent vectors at bifurcation points of continuation curves that define the boundary of manipulator workspaces. A cross-section of the workspace is performed and boundary continuation curves are traced. The method was demonstrated for a closed-loop mechanism called the Stewart Platform [9]. Although Haug's method can be used to determine the wrist workspace, there are many characteristics to that method that renders it inapplicable to the goal of this paper. If Haug's method is used, it would produce the workspace numerically. The workspace needed in our formulation requires an analytical representation of the wrist workspace.

More recently, an algebraic formulation to determine the workspace of four-revolute manipulators was presented by Cecarelli and Vinciquerra [10]. The benefit of this method is the ability to determine holes and voids in the workspace. Dexterity of manipulators was studied by

Yang and Lee [11], Yang and Lai [12], Lai and Menq [13], Wang and Wu [14], and Emiris [15]. Studies of workspace and dexterity of parallel manipulators are reported by Agrawal [16] and Gosselin and Angeles [17]. Pennock and Kassner [18] developed a general method for determining the workspace of three-degree-of-freedom planar manipulators.

Prior to these aforementioned works, there have been many works that have dealt with the general subject of manipulator workspaces. The reciprocal screw method for workspace generation, for example, is based on the fact that when the end-effector reference point of the manipulator is on the workspace boundary, all the joint axes of a manipulator are reciprocal to a zero pitch wrench axis [19]. For each degree-of-freedom lost, there exists one reciprocal screw which, if applied as a wrench to the end-effector, produces no virtual work for the manipulator joints. Wang and Waldron [20], based upon earlier work [21], stated that as the Jacobian of the manipulator becomes singular if its columns, which are screw quantities, do not span the full rank of the matrix, therefore reducing the Jacobian rank by at least one.

Other methods that are based on a Jacobian's singularity can also be found in [22-24]. An enumeration of singular configurations due to the vanishing of the determinant of the Jacobian and the Jacobian's minors is presented by Lipkin and Pohl [25]. Shamir [26] provided an analytical tool to determine if the singularities are avoidable for three degree-of-freedom manipulators. Gorla [27] reported obtaining expressions for the set of singular points by assuming that link twists were multiple of $\pi/2$. Other earlier important studies that discussed manipulator singularities include Soylu and Duffy [28] and Lai and Yang [29].

Early studies that have addressed difficulties in the control of manipulators due to the appearance of interior curves and surfaces were reported by Waldron [30] and Nielsen et al. [31]. In the latter work, the controllability of a mechanical arm is discussed from a differential geometry point of view.

The objective of this paper is to analytically determine the surfaces enveloping the wrist workspace of a defined point in a six-degree-of-freedom mechanism. In the following discussion, the criteria for determining singular surfaces will be first presented in Section 3. Singular surfaces will be used to numerically trace singular curves using numerical algorithms. The discussion of determining tangents at bifurcation points is not presented in this paper but is addressed in recent work by Abdel-Malek and Yeh [32] based upon a singularity method developed by Lucaks [33]. Section 3 discusses a numerical method for determining the intersection between singular curves such that subsurfaces are defined. A perturbation method is used to select those surfaces that are boundary to the wrist workspace. Section 4 presents the development of atlases by intersecting these subsurfaces with the service sphere and projecting solutions onto an atlas. A planar example is presented in Section 5 and a spatial example in Section 6.

2. Problem Formulation

In order to obtain an atlas of orientability at a target, it is necessary to:

(1) Develop a systematic method to determine boundary surfaces to the wrist workspace.

(2) Intersect the service sphere with the boundary to the wrist workspace to determine service regions. To compute these intersections, it is necessary that the boundary be analytic.

(3) Determine service regions due to constraints imposed on distal joints.

(4) Project the intersections onto maps depicting orientability

The service sphere is used to indicate all possible orientations penetrating through its surface to the target. A manipulator having at most six degrees of freedom can be modeled using the Denavit-Hartenberg representation method [34]. A point located on either link two or three will be referred to as the wrist point. Links subsequent to the wrist point will be referred to as distal links. Thus a manipulator is partitioned into two segments; links before the wrist point and links after the wrist point. The position vector in terms of joint coordinates of a wrist point for a serial manipulator arm can be written as

$$\begin{bmatrix} \mathbf{x}(\mathbf{q}) \\ 1 \end{bmatrix} = {}^{0}\mathbf{T}_{3}(\mathbf{q}) \begin{bmatrix} {}^{3}\mathbf{x}_{w} \\ 1 \end{bmatrix} \tag{1}$$

where $\mathbf{q} = [q_1, q_2, q_3]^T \in R^3$ is the vector of generalized joint coordinates for the three-degree-of-freedom mechanism used for positioning the wrist point, ${}^{0}\mathbf{T}_{3}(\mathbf{q}) = \begin{bmatrix} {}^{0}\mathbf{R}_{3} & {}^{0}\mathbf{p}_{3} \\ \mathbf{0} & 1 \end{bmatrix}$ is the (4×4) homogeneous transformation matrix, ${}^{0}\mathbf{p}_{3}$ is the position vector from the reference frame to the wrist point, and ${}^{0}\mathbf{R}_{3}$ is the (3×3) rotation matrix. The Denavit-Hartenberg representation allows for forming the transformation between two successive links by substituting in the homogeneous transformation matrix

$${}^{i-1}\mathbf{T}_{i} = \begin{bmatrix} \cos\theta_i & -\cos\alpha_i \sin\theta_i & \sin\alpha_i \sin\theta_i & a_i \cos\theta_i \\ \sin\theta_i & \cos\alpha_i \cos\theta_i & -\sin\alpha_i \cos\theta_i & a_1 \sin\theta_i \\ 0 & \sin\alpha_i & \cos\alpha_i & d_i \\ 0 & 0 & 0 & 1 \end{bmatrix} \tag{3}$$

where θ_i is the joint angle from $\mathbf{x}_{i-1}$ to the $\mathbf{x}_i$ axis, d_i is the distance from the origin of the *(i-1)*th coordinate frame to the intersection of the $\mathbf{z}_{i-1}$ axis with the $\mathbf{x}_i$, a_i is the offset distance from the intersection of the $\mathbf{z}_{i-1}$ axis with the $\mathbf{x}_i$ axis, and α_i is the offset angle from the $\mathbf{z}_{i-1}$

axis to the $\mathbf{z}_i$ axis. A transformation matrix between link 0 and link i is the successive multiplication of intermediate matrices such that ${}^0\mathbf{T}_i = {}^0\mathbf{T}_1\,{}^1\mathbf{T}_2 \ldots {}^{i-1}\mathbf{T}_i = \prod_{j=1}^{i} {}^{j-1}\mathbf{T}_j$.

The position vector describing the coordinates of the wrist point can be written as

$$\mathbf{x}(\mathbf{q}) = {}^0\mathbf{R}_3(\mathbf{q})\,{}^3\mathbf{x}_w + {}^0\mathbf{p}_3(\mathbf{q}) \tag{2}$$

At a certain position in space, the generalized coordinates satisfy independent holonomic kinematic constraint equations of the form

$$\Phi(\mathbf{q}) = \mathbf{x}(\mathbf{q}) - {}^0\mathbf{R}_3(\mathbf{q})\,{}^3\mathbf{x}_w - {}^0\mathbf{p}_3(\mathbf{q}) = 0 \tag{3}$$

where ${}^3\mathbf{x}_w$ is the vector describing the wrist point resolved in the reference frame of link 3.

The method formulated in this paper is applicable to manipulators having up to six degrees of freedom with revolute and prismatic joints.

3. A Systematic Method for Determining the Boundary to the Wrist Workspace

In order to find the analytical boundary to the wrist workspace, the kinematics of the underlying mechanism will be formulated. First-order singularities defined in the context of this paper are the values of generalized coordinates that make the Jacobian singular. It is the value of a generalized coordinate that causes the mechanism to lose at least one degree of mobility. In order to find analytical expressions for the boundary to the wrist workspace, it is necessary to (1) determine singular surfaces due to first-order singularities, (2) determine singular curves that partition singular surfaces to subsurfaces, and (3) determine which of these subsurfaces are on the boundary.

3.1 Parametrization of Singular Surfaces

First-order singularities are computed by equating the determinant of the Jacobian of the mechanism to zero and computing its roots. The constraint Jacobian of the constraint function $\Phi(\mathbf{q})$ for a certain configuration $\mathbf{q}^0$ is the 3×3 matrix

$$\Phi_{\mathbf{q}}(\mathbf{q}^0) = \left[\frac{\partial \Phi_i}{\partial q_j}\left(\mathbf{q}^0\right) \right] \tag{4}$$

To impose joint limits of actuators in terms of the generalized variables, it is possible to transform a constraint of the form

$$q_i{}^{\min} \le q_i \le q_i{}^{\max} \qquad\qquad i = 1,2,3 \tag{5}$$

into an equation by introducing a new generalized coordinate λ_i such that the inequality constraint can be rewritten as

$$q_i = a_i + b_i \sin \lambda_i \tag{6}$$

where $a_i = \left(q_i{}^{\max} + q_i{}^{\min}\right)/2$ and $b_i = \left(q_i{}^{\max} - q_i{}^{\min}\right)/2$ are the mid-point and half-range of the inequality constraint. Thus, the Jacobian with respect to the new coordinates $\lambda = \begin{bmatrix} \lambda_1 & \lambda_2 & \lambda_3 \end{bmatrix}$ can be written as

$$\Phi_\lambda = \frac{\partial \Phi_i}{\partial q_j}\frac{\partial q_j}{d\lambda_j} = \Phi_{\mathbf{q}}\mathbf{q}_\lambda \tag{7}$$

Singularities are determined by equating the determinant of Φ_λ to zero such that

$$\mathbf{F}(\lambda) = \left|\Phi_{\mathbf{q}}\mathbf{q}_\lambda\right| = \mathbf{0} \tag{8}$$

Solutions to Eq. (8) are values for λ that are substituted into Eq. (2) to obtain singularities in terms of the generalized coordinates $\mathbf{q}$.

Substituting a singularity into Eq. (2) results in a function describing a parametric surface (two parameters) called a singular surface. For example, if a singularity occurs at $q_1 = constant$, the surface resulting from substituting q_1 into Eq. (2) will be parametrized as $\mathbf{x}^n(q_2, q_3)$, where *n* indicates the surface number. Singular surfaces are two-dimensional in three-dimensional space, generated by having one of the generalized coordinates be a constant (a singularity). These surfaces are barriers to motion of the wrist point.

These surfaces may exist inside the wrist workspace, on the outer surface, or may extend to be both internal and external to the wrist workspace. Singular surfaces may intersect each other

resulting in intersection curves called singular curves. These curves between singular surfaces determine a different type of singularity, which divide a singular surface into a number of subsurfaces. The set of generalized coordinates (two constant generalized coordinates) resulting from this intersection are called second-order singularities. In the analysis that follows, it is necessary to determine these curves and their intersection. It is not necessary, however, to determine the value of the second-order singularity.

3.2 Singular Curves

In order to determine the intersection between two parametric surfaces, one parametrized as

$$\mathbf{x}^i(q_1,q_2)={}^0\mathbf{R}_3(q_1,q_2,constant)\,{}^3\mathbf{x}_w+{}^0\mathbf{p}_3$$

and the other parametrized as

$$\mathbf{x}^j(t_1,t_2)={}^0\mathbf{R}_3(t_1,t_2,constant)\,{}^3\mathbf{x}_w+{}^0\mathbf{p}_3$$

a solution to the following equation is necessary:

$$\mathbf{x}^i(q_1,q_2)-\mathbf{x}^j(t_1,t_2)=\mathbf{0} \tag{9}$$

subject to inequality constraints imposed on the joints in the form of Eq. (5). Thus Eq. (8) can be augmented by the inequality constraints as

$$\mathbf{H}(\mathbf{s})=\begin{bmatrix}\mathbf{x}^1(q_1,q_2)-\mathbf{x}^2(t_1,t_2)\\ q_1-a_1-a_2\sin\lambda_1\\ q_2-b_1-b_2\sin\lambda_2\\ t_1-c_1-c_2\sin\lambda_3\\ t_2-d_1-d_2\sin\lambda_4\end{bmatrix}=\mathbf{0} \tag{10}$$

where $\mathbf{s}$ is the extended vector defined as $\mathbf{s}=\begin{bmatrix}q_1 & q_2 & t_1 & t_2 & \lambda_1 & \lambda_2 & \lambda_3 & \lambda_4\end{bmatrix}^T$. Since the Jacobian of $\mathbf{H}(\mathbf{s})$ is not square, the problem of obtaining an initial solution (initial point) can be solved using the Moore-Penrose pseudo inverse [35]. The new generalized coordinates are calculated by evaluating

$$\Delta\mathbf{s}=\mathbf{H}_\mathbf{s}^*(-\mathbf{H}) \tag{11}$$

where $\mathbf{H}_\mathbf{s}^*$ is the Moore-Penrose pseudo inverse of the Jacobian $\mathbf{H}_\mathbf{s}=\left[\partial H_i/\partial s_j\right]$, defined by

$$\mathbf{H}_\mathbf{s}^*=\mathbf{H}_\mathbf{s}^T\left(\mathbf{H}_\mathbf{s}\mathbf{H}_\mathbf{s}^T\right)^{-1} \tag{12}$$

This method converges within a few iterations without adding any new constraints [35]. Another method for determining a staring point for a surface-surface intersection problem was developed by Muellenheim [36]. Once a starting point is found, the intersection curve is traced along the tangent direction by using the so-called marching method developed by Pratt and Geisow [37]. Other numerical methods that can be used for this purpose can be found in Keller [38] and Rheinboldt [39]. The algorithm requires a vector tangent direction to compute marching parameters. Let $\mathbf{x}^1_{q_1}$ denote the derivative of $\mathbf{x}^1$ with respect to q_1 and $\mathbf{x}^1_{q_2}$ denote the derivative of $\mathbf{x}^1$ with respect to q_2. The cross-product of these vectors result in a normal to the surface such that

$$\mathbf{n}^1 = \left(\mathbf{x}^1_{q_1} \times \mathbf{x}^1_{q_2}\right) / \left\|\mathbf{x}^1_{q_1} \times \mathbf{x}^1_{q_2}\right\| \tag{13}$$

Similarly, the normal at a point on the second surface is defined by

$$\mathbf{n}^2 = \left(\mathbf{x}^2_{t_1} \times \mathbf{x}^2_{t_2}\right) / \left\|\mathbf{x}^2_{t_1} \times \mathbf{x}^2_{t_2}\right\| \tag{14}$$

The tangent vector τ is computed as

$$\boldsymbol{\tau} = \mathbf{n}^1 \times \mathbf{n}^2 \tag{15}$$

The new step constraint equation can be written as

$$[\mathbf{x}^1(q_1, q_2) - \mathbf{x}^o] \cdot \boldsymbol{\tau} - c = 0 \tag{16}$$

where $\mathbf{x}^o$ is the computed point, and c is the step size.

Although this method will converge, it is possible to find only one starting point, and thus only one corresponding branch of intersection will be traced. The problem of numerically determining the intersection curve is complicated when several curves exist. In that case, tangents at bifurcation points have to be computed.

The physical significance of singular curves stems from having two constant generalized coordinates. i.e., the manipulator loses at least two degrees of mobility. These singular curves

partition singular surfaces into a number of regions called subsurfaces denoted by Ψ^i. For a singular surface, the intersection of curves c^k results in nodes n^j. For example, to determine subsurfaces on surface $\mathbf{x}^3$ in Fig. (1a), it is intersected with $\mathbf{x}^2$ and $\mathbf{x}^1$ to determine singular curves. The singular curves are superimposed on surface $\mathbf{x}^3$ as depicted in Fig. (1b). The curves partition this surface to four subsurfaces each bounded by curve segments. These intersections were found by using a rectangular grid as shown in Fig. (1c). Two curves are checked whether they exist inside an incremental rectangle. The tolerance (rectangle width) is subsequently decreased. Difficulties in computing the intersection of singular curves may arise if the curves are intersecting at more than one point (along a segment).

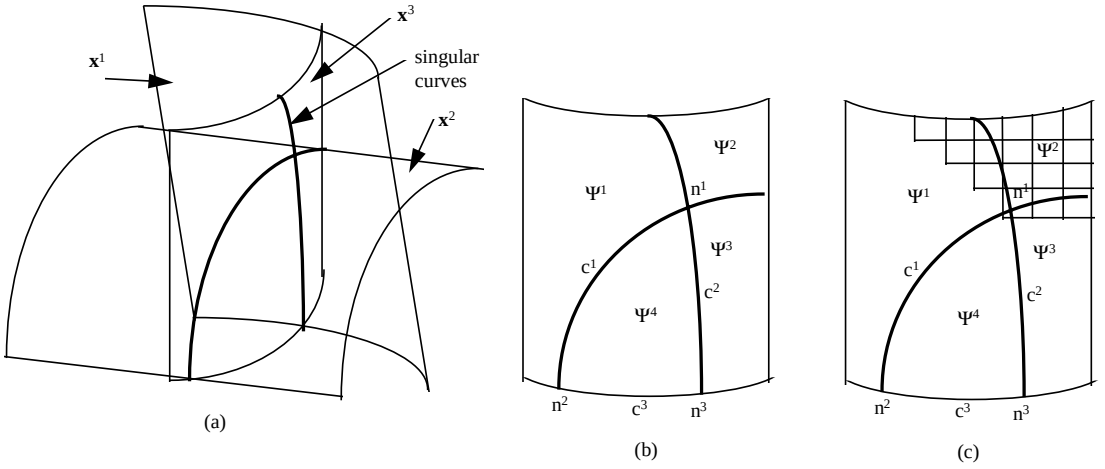

Fig. 1 (a) Intersection of singular surfaces (b) Partitioning of a singular surface to subsurfaces

Subsurfaces due to internal, boundary, and higher-order singularities are computed. It remains to be determined whether these subsurfaces are internal or boundary surfaces. This can be performed by perturbing a known point on the subsurface and determining whether the perturbed points satisfy the constraint equation. Any point can be chosen, provided that it is not on the boundary of the subsurface. For subsurface $\Psi^i(\mathbf{q})$, the partial derivatives with respect to the parametrization variables q_1 and q_2 are $\partial\Psi^i/\partial q_1$ and $\partial\Psi^i/\partial q_2$. At any regular point $\mathbf{q}^o$ on the subsurface, these vectors are linearly independent and tangent to the coordinate curves through $\mathbf{q}^o$ (they span the tangent plane of $\Psi^i(\mathbf{q})$ at $\mathbf{q}^o$). The unit vector $\hat{\mathbf{n}}$, which is orthogonal to those vectors, is

$$\hat{\mathbf{n}}(\mathbf{q}^o) = \frac{\left(\dfrac{\partial \Psi^i}{\partial q_1} \times \dfrac{\partial \Psi^i}{\partial q_2}\right)}{\left\| \dfrac{\partial \Psi^i}{\partial q_1} \times \dfrac{\partial \Psi^i}{\partial q_2} \right\|} \tag{17}$$

For a small perturbation $\partial\varepsilon$ about the point $\mathbf{q}^o$ and along the normal $\hat{\mathbf{n}}(\mathbf{q}^o)$, the coordinates of the perturbed points are

$$\mathbf{x}_{1,2}(\mathbf{q}^o) = \Psi^i(\mathbf{q}^o) \pm \partial\varepsilon\hat{\mathbf{n}}(\mathbf{q}^o) \tag{18}$$

If the perturbed point is inside the wrist workspace, it has to satisfy the constraint equation (Eq. 3), subject to inequality constraints of Eq. (6). Substituting Eq. (18) into Eq. (3) and augmenting the system of equations with the parametrized inequality constraints, the perturbed point is inside if there exists a solution to the following system of equations:

$$\begin{bmatrix} {}^0\mathbf{R}_3\,{}^3\mathbf{x}_w + {}^0\mathbf{p}_3 - \Psi^i(\mathbf{q}^o) \mp \partial\varepsilon\hat{\mathbf{n}}(\mathbf{q}^o) \\ q_1 - b_1 - c_1 \sin\lambda_1 \\ q_2 - b_2 - c_2 \sin\lambda_2 \\ q_3 - b_3 - c_3 \sin\lambda_3 \end{bmatrix} = \mathbf{0} \tag{19}$$

Solutions to both perturbation points indicates that the subsurface is internal. *Thus, a subsurface* $\Psi^i(\mathbf{q})$ *is internal if and only if there exists a solution for Eq. (19) for both perturbations* $\pm\partial\varepsilon$. Subsurfaces that are boundary to the wrist workspace are then used to construct the boundary to the wrist workspace.

4. Determining Service Regions

At a target in the workspace (e.g., a malignant tumor in the head) the center of the service sphere is located. Figure 2 depicts a service sphere located at a target.

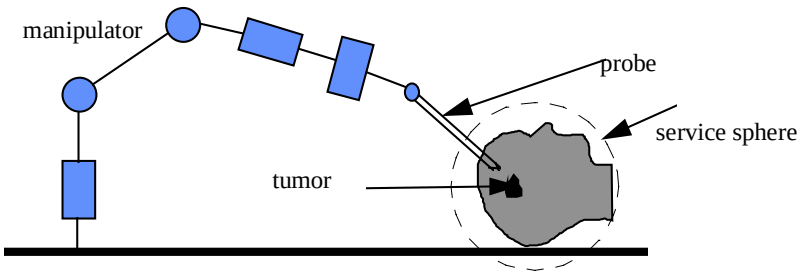

Fig. 2 A Service Sphere Located at a Target

The wrist point **w** is allowed to exist inside the wrist workspace determined in the previous section. This point **w** is also allowed to exist inside a different region that is generated by distal joints and links. Boundary surfaces to these two regions will be intersected. Curves of intersection will be computed. Regions formed by these curves indicate all possible positions for the wrist point to exist.

For example, Fig. (3a) depicts a six-degree-of-freedom manipulator. The wrist point **w** will be assumed to be located at the end of the third joint. For the wrist point **w**, the methods of Section 3 are used to develop the boundary to the wrist workspace shown in Fig. (3b). For the joints 4, 5, and 6, assuming a spherical joint at the point **p**, the point **w** maps the volume between two concentric spheres as shown in Fig. (3c).

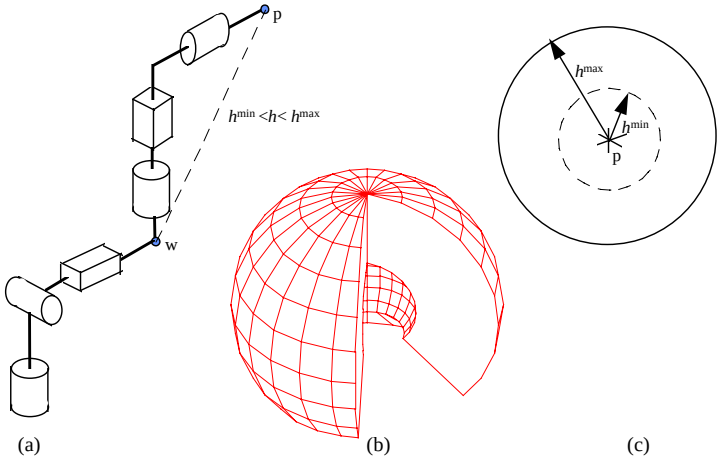

Fig. 3 (a) A Six Degree-of-freedom Manipulator (b) Wrist Workspace (c) Service sphere

4.1 Service Regions Due to Wrist Workspace

To determine service regions at an operating point **p**, a service sphere parametrized as $\mathbf{x}_{ss}(u,v) = \mathbf{p} + \left[h\cos v\cos u \quad h\cos v\sin u \quad h\sin v\right]^T$, is located with center at **p** and radius h (h is the distance between point **p** on the end-effector and the wrist point **w**). The wrist point

assumes a position on the surface of the service sphere and has to satisfy Eq. (3). Using this definition, the service region is defined as the set of points on the surface of the service sphere and inside the wrist workspace. The service region $SR_i(\mathbf{p},\mathbf{q})$ is a set that exists on the surface of the service sphere such that

$$SR_i(\mathbf{p},\mathbf{q}) = \{\mathbf{x}_{ss}(u,v) = \mathbf{0},\ \textit{for some}\ \mathbf{q}\} \tag{20}$$

and belongs to the wrist workspace such that

$$SR_i(\mathbf{p},\mathbf{q}) = \{\Phi(\mathbf{q}) = \mathbf{0},\ \textit{for some}\ \mathbf{q}\} \tag{21}$$

Since the boundary of the wrist workspace has been *analytically* determined, it is possible to intersect each subsurface with the service sphere to determine the intersection curve. To determine whether the service region is enclosed by the intersecting curve or lies outside it, a ray is cast in the direction of the normal passing through $\mathbf{p}$. The ray will intersect the sphere in two points $\mathbf{s}_1$ and $\mathbf{s}_2$. The service region is identified by determining which of these points satisfies the local constraint equation. A local constraint equation accounts for the inequality constraint associated with the singularity of the subsurface. The intersection curve is the set of solutions to Λ_1, such that

$$\Lambda_1 = \begin{bmatrix} \Psi^i(\mathbf{q}) - \mathbf{x}_{ss}(u,v) \\ q_i - a_i - b_i \sin\lambda_i \end{bmatrix} = \mathbf{0} \tag{22}$$

The service region is identified by determining one of the points on the ray satisfying the following

$$\Lambda_2 = \begin{bmatrix} \Psi^i(\mathbf{q}) + t\hat{\mathbf{n}}(\mathbf{p}) - \mathbf{x}_{ss}(u,v) \\ q^{local} - a - b\sin\lambda \end{bmatrix} = \mathbf{0} \tag{23}$$

Numerical solutions to Eq. (25) are obtained. To visualize service regions, it is convenient to project these service regions onto two dimensional maps. The intersection curve of each subsurface with the service sphere is parametrized in terms of parameters *u* and *v* on the surface of the sphere.

4.2 Constraints Due to Distal Links

Service regions due to distal links of a manipulator are considered. In the previous analysis, inequality constraints of the links prior to the wrist point were considered in determining the boundary to the wrist workspace. Service regions will be determined by computing limiting positions of the wrist point for an assembled configuration. For example, for a four-degree-of-freedom manipulator and a wrist point located on the third link, two limiting positions of the wrist point are computed for $q_4 = q_4^{\min}$ and for $q_4 = q_4^{\max}$, where q_4 is the generalized coordinate of joint four. For a five-degree-of-freedom manipulator with a wrist point on the third link, there are four limiting positions for the wrist such that: $(q_4^{\min}, q_5^{\min})$, $(q_4^{\min}, q_5^{\max})$, $(q_4^{\max}, q_5^{\min})$, and $q_4^{\max}, q_5^{\min}$. For a six degree-of-freedom manipulator with the end-effector at a target point **p**, the mechanism is assembled and the constraint equation is

$$\begin{bmatrix} \mathbf{p} \\ 1 \end{bmatrix} = {}^0\mathbf{T}_4(q_1, q_2, q_3, q_4)\,{}^4\mathbf{T}_6(q_5, q_6)\begin{bmatrix} {}^6\mathbf{x}_e \\ 1 \end{bmatrix} \tag{24}$$

where ${}^0\mathbf{T}_4 = \left[\begin{array}{c|c} {}^0\mathbf{R}_4 & {}^0\mathbf{p}_4 \\ \hline \mathbf{0} & 1 \end{array}\right]$, ${}^4\mathbf{T}_6 = \left[\begin{array}{c|c} {}^4\mathbf{R}_6 & {}^4\mathbf{p}_6 \\ \hline \mathbf{0} & 1 \end{array}\right]$, and ${}^6\mathbf{x}_E$ is the vector describing a point on the end-effector with respect to link 6. Equation (24) can be expanded in terms of three equations as

$$\mathbf{p} = {}^0\mathbf{R}_4({}^4\mathbf{R}_6\,{}^6\mathbf{x}_E + {}^4\mathbf{p}_6) + {}^0\mathbf{p}_4 \tag{25}$$

Recognizing that the wrist point coincides with the origin of the fourth reference frame, the wrist point can be calculated as

$$\mathbf{w} = \mathbf{p} - {}^0\mathbf{R}_4({}^4\mathbf{R}_6\,{}^6\mathbf{x}_E + {}^4\mathbf{p}_6) \tag{26}$$

The spherical wrist is constrained as

$$q_4^{\min} \le q_4 \le q_4^{\max} \tag{27a}$$

$$q_5^{\min} \le q_5 \le q_5^{\max} \tag{27b}$$

$$q_6^{\min} \le q_6 \le q_6^{\max} \tag{27c}$$

At any combination of the above joint limits, the coordinates of the wrist point is well defined for eight configurations (eight combinations of q_4, q_5, q_6).

Curves connecting two wrist points $\mathbf{w}_i$ and $\mathbf{w}_j$ can be computed as follows. A local coordinate system is formed with origin at $\mathbf{p}$ and extending its x-axis from $\mathbf{w}_i$ to $\mathbf{p}$ such that $\mathbf{x}_l = \mathbf{w}_i - \mathbf{p}$. A vector in the local xy-plane is calculated as $\mathbf{v}_l = \mathbf{w}_j - \mathbf{p}$. The normal to the local plane is $\mathbf{z}_l = \mathbf{x}_l \times \mathbf{v}_l$. Thus, the rotation matrix relating the local reference frame to the zeroth reference frame is computed as

$$^0\mathbf{R}_l = \left[\mathbf{x}_l \;\vdots\; \mathbf{z}_l \times \mathbf{x}_l \;\vdots\; \mathbf{x}_l \times \mathbf{v}_l\right] \tag{28}$$

Points on the curve connecting the two wrist points are computed by transforming points generated on the surface such as

$$\mathbf{w}_i = {}^0\mathbf{R}_l \left[h\cos\phi_i \quad h\sin\phi_i \quad 0\right]^T + \mathbf{p} \tag{29}$$

These curves enclose regions on the service sphere. To determine whether these regions are service regions, a point inside the region is studied such that the inverse kinematic solutions are obtained that satisfy the inequality constraints. Resulting service regions due to distal links are superimposed on service regions due to the first three joints. The resulting map is an atlas of orientability.

5. Planar Example

Consider the three-degree-of-freedom manipulator depicted in Fig. (4). Let the wrist point **w** coincide with the axis of rotation of the third joint. Thus, the distal joint is link 3. In this example, the wrist workspace will first be determined, the effect of constraint of the distal joint will be taken into consideration, and finally atlases of orientability will be developed.

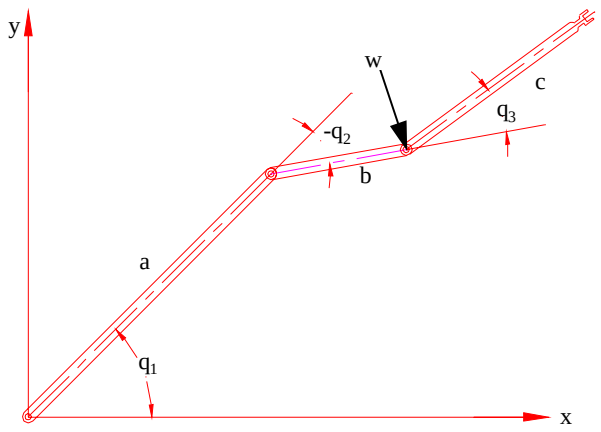

Fig. 4 A Three-Degree-of-Freedom Planar Manipulator

To illustrate the methodology, let $a = 5$, $b = 2$, and $c = 3$. Each joint is constrained as follows.

$$-45^o \le q_1 \le 135^o \tag{30a}$$

$$-150^o \le q_2 \le 120^o \tag{30b}$$

$$-120 \le q_3 \le 30^o \tag{30c}$$

To determine analytical boundary of the wrist point (boundary to the wrist workspace), the position vector of the wrist point is formulated as

$$\mathbf{x} = \begin{bmatrix} 5\cos q_1 + 2\cos(q_1 + q_2) \\ 5\sin q_1 + 2\sin(q_1 + q_2) \end{bmatrix} \tag{31}$$

subject to the inequality constraints of Eq. (3). These constraints are parametrized as follows.

$$q_1 = \frac{\pi}{2} + \pi \sin \lambda_1 \tag{32a}$$

$$q_2 = -\frac{\pi}{6} + \frac{3\pi}{2} \sin \lambda_2 \tag{32b}$$

$$q_3 = -\frac{\pi}{2} + \frac{5\pi}{6} \sin \lambda_3 \tag{32c}$$

The holonomic kinematic constraints are formed from Eq. (31) such that

$$\Phi(\mathbf{q}) = \begin{bmatrix} x - 5\cos q_1 + 2\cos(q_1 + q_2) \\ y - 5\sin q_1 + 2\sin(q_1 + q_2) \end{bmatrix} \tag{33}$$

To determine the Jacobian with respect to the new parameters λ_i, the two matrices $\mathbf{\Phi_q}$ and $\mathbf{q}_\lambda$ of Eq. (8) are evaluated

$$\mathbf{\Phi_q} = \begin{bmatrix} -a\sin q_1 - b\sin(q_1 + q_2) & -b\sin(q_1 + q_2) \\ a\cos q_1 + b\cos(q_1 + q_2) & b\cos(q_1 + q_2) \end{bmatrix} \tag{34}$$

$$\mathbf{q}_\lambda = \begin{bmatrix} \pi\cos\lambda_1 & 0 \\ 0 & \frac{3}{2}\pi\cos\lambda_2 \end{bmatrix} \tag{35}$$

The determinant of the Jacobian is evaluated such that

$$\left|\Phi_{\mathbf{q}}\mathbf{q}_\lambda\right| = 3.701(a)(b)\cos\lambda_1\cos\lambda_2\sin\left(0.262 - 2.356\sin\lambda_2\right) \tag{36}$$

To determine singularities, the determinant of the Jacobian is equated to zero. The term $\cos\lambda_1$ equals zero if $\lambda_1 = -\frac{\pi}{2}$ or $\frac{\pi}{2}$. Substituting λ_1 into Eq. (32a) yields two singularities: $q_1 = -45^o$ and $q_1 = 135^o$. Similarly, the term $\cos\lambda_2$ equals zero if $\lambda_2 = -\frac{\pi}{2}$ or $\frac{\pi}{2}$. Substituting λ_2 into Eq. (32b) yields two singularities: $q_2 = -150^o$ and $q_2 = 120^o$. Finally, the term $\sin\left(0.262 - 2.356\sin\lambda_2\right)$ equals zero if $0.262 - 2.356\sin\lambda_2 = 0$ or π. The left hand side is equal to q_2, hence, two additional singularities are considered $q_2 = 0, \pi$. However, because $q_2 = \pi$ is not within the joint limits, it is not considered. There are a total of five singularities.

Each singularity is substituted into the position vector equation (Eq. 31) to generate singular surfaces. In the planar case, these surfaces are reduced to singular curves. For example, substituting the singularity $q_2 = 120^o$ into Eq. (31) yields a singular curve $\mathbf{x}_2$ (an arc) parametrized as

$$\mathbf{x}_2 = \begin{bmatrix} 5\cos q_1 + 2\cos(q_1 + 120^0) \\ 5\sin q_1 + 2\sin(q_1 + 120^0) \end{bmatrix} \tag{37}$$

subject to the inequality constraint $-45^o \le q_1 \le 135^o$. The five singular curves are shown in Fig. (5).

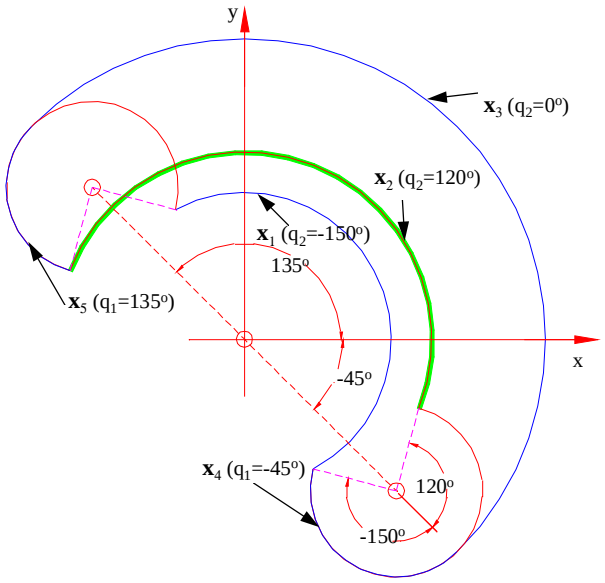

Fig. 5 Singular Curves

Part of the singular curve $\mathbf{x}_2$ is on the boundary and part of it is inside the workspace. To determine which singular curves are boundary to the workspace, each curve is intersected with all other curves. The perturbation method is then used to eliminate singular curves that are inside the wrist workspace. For example, the singular curve $\mathbf{x}_2$ is intersected with $\mathbf{x}_5$ such that $\mathbf{x}_2$ is partitioned into Ψ_1 and Ψ_2 as shown in Fig. (6).

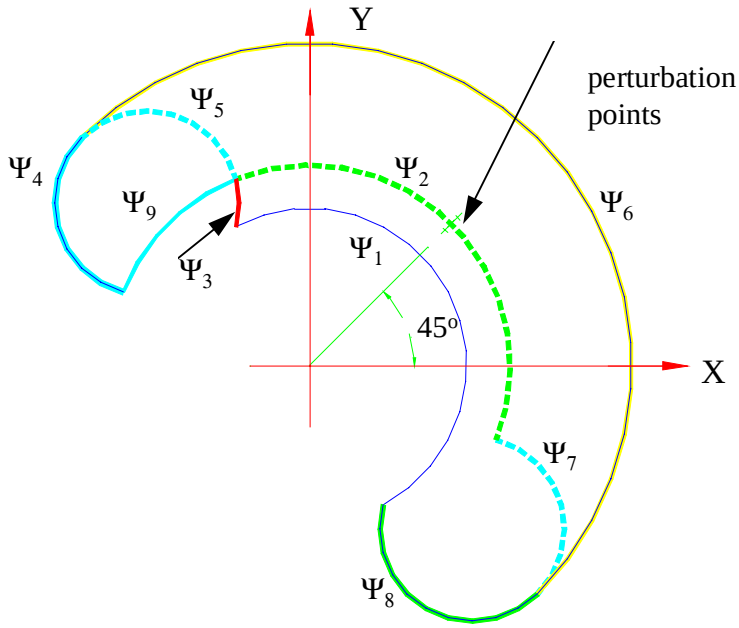

Fig. 6 Partitioning of Singular Curves

Consider a point on the curve Ψ_2 in the middle of its interval (i.e., $q_1 = 45^o$). The coordinates of the first perturbation point are calculated as

$$\mathbf{p}_1 = \Psi_2 + \varepsilon\hat{\mathbf{n}} = \begin{bmatrix} 1.674 & 4.053 \end{bmatrix}^T \tag{38a}$$

where $\varepsilon = 0.1$ and $\hat{\mathbf{n}} = \begin{bmatrix} \cos q_1 & \sin q_1 \end{bmatrix}^T$. An inverse solution can be found for $\mathbf{p}_1$ such that $q_1 = 44.385^o$ and $q_2 = 117.356^o$. The coordinates of the second perturbation point for Ψ_2 are

$$\mathbf{p}_2 = \Psi_2 - \varepsilon\hat{\mathbf{n}} = \begin{bmatrix} 1.533 & 3.982 \end{bmatrix}^T \tag{38b}$$

An inverse solution can be found for $\mathbf{p}_2$ such that $q_1 = 92.186^o$ and $q_2 = -122.662^o$. Thus, this singular curve is a boundary to the wrist workspace and is indicated using a dotted line.

The process is repeated for all segments of each singular curve. Segments of singular curves that are boundary to the wrist workspace are depicted as solid lines in Fig. (6). At a point $\mathbf{p} = \begin{bmatrix} 4.691 & 1.155 \end{bmatrix}^T$ in the reachable workspace, it is required to develop an atlas of orientability. The independent holonomic constraint for this manipulator is

$$\Phi = \begin{bmatrix} x - a\cos q_1 - b\cos(q_1 + q_2) - c\cos(q_1 + q_2 + q_3) \\ y - a\sin q_1 - b\sin(q_1 + q_2) - c\sin(q_1 + q_2 + q_3) \end{bmatrix} = \mathbf{0} \tag{39}$$

To determine the configuration of the manipulator (wrist position) for a given generalized coordinate q_3, the service sphere is located at $\mathbf{p}$ with radius equal to the length of the distal link (the length is $c=3$). For $q_3 = q_3^{\min} = -120^0$, a solution is sought to

$$\begin{bmatrix} p_x - a\cos q_1 - b\cos(q_1 + q_2) - c\cos(q_1 + q_2 - 120^o) \\ p_y - a\sin q_1 - b\sin(q_1 + q_2) - c\sin(q_1 + q_2 - 120^o) \end{bmatrix} = \mathbf{0} \tag{40}$$

There exists a solution to Eq. (40) such that $q_1 = 44.995^o$ and $q_2 = -30.001^o$. The manipulator is shown in this configuration in Fig. 7. Similarly, for $q_3 = q_3^{\max} = 30^0$, the joint angles are $q_1 = -45.078^o$ and $q_2 = 103.13^o$ also shown in Fig. 7. The arc connecting the two limiting positions $\mathbf{w}_1$ and $\mathbf{w}_2$ is shown in Fig. 7.

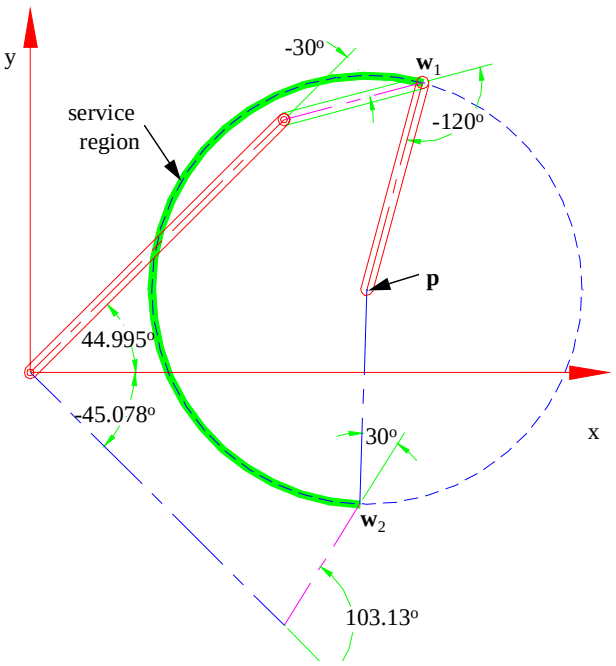

Fig. 7 Service Region Due to a Distal Joint

The service region due to the distal joints is superimposed on the wrist workspace. Since the wrist can only exist inside the wrist workspace and on the service region, only those regions that are common to both are considered. These regions (depicted as arcs) are shown in Fig. (8a). A one dimensional map of orientability for this planar manipulator is shown in Fig. 8b by unrolling the service circle onto a line. Service regions (shown using a thicker line in Fig. 8a) are shown as shaded in Fig. 8b.

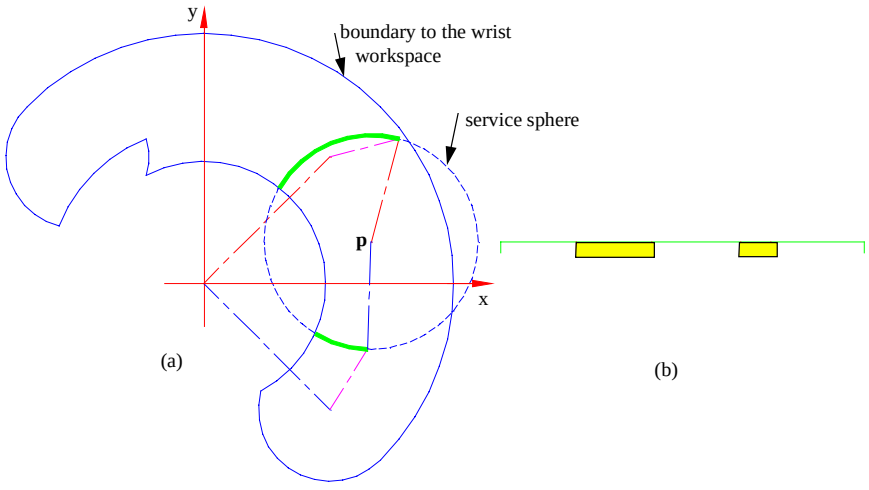

Fig. 8 (a) Superimposing the wrist workspace with service regions due to distal links (b) A one dimensional atlas of orientability

6. Spatial Example

Consider the six degree-of-freedom (all revolute joints) manipulator depicted in Fig. (9) with the following geometry $d_1 = 50$, $d_3 = 10$, $d_4 = 25$, $d_6 = 10$, and $a_2 = 20$. Consider the first three axis as being the positioning mechanism for the spherical wrist with w being the wrist point. Boundary surfaces to the wrist workspace for the wrist point at ${}^3\mathbf{x}_w = \begin{bmatrix} 0 & 0 & d_4 \end{bmatrix}^T$ will be studied.

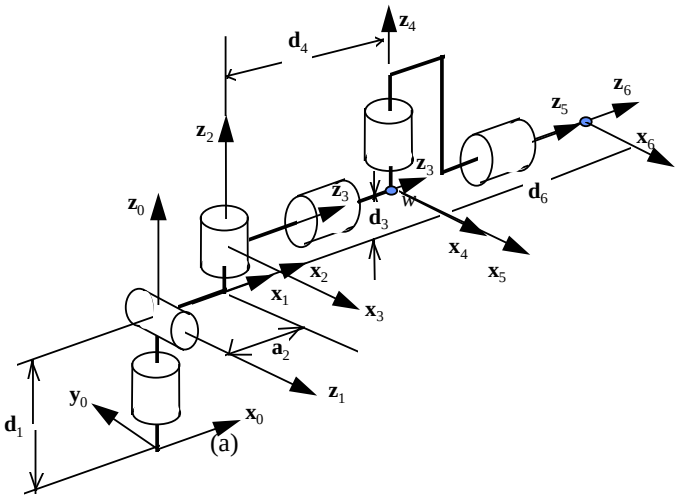

Fig. 9 A six degree-of-freedom manipulator

For this manipulator, the three homogeneous transformation matrices using the Denavit-Hartenberg representation of joints 1, 2, and 3 are

$$ {}^0\mathbf{T}_1 = \begin{bmatrix} \cos q_1 & 0 & \sin q_1 & 0 \\ \sin q_1 & 0 & -\cos q_1 & 0 \\ 0 & 1 & 0 & 50 \\ 0 & 0 & 0 & 1 \end{bmatrix} \tag{41} $$

$$ {}^1\mathbf{T}_2 = \begin{bmatrix} \cos q_2 & 0 & -\sin q_2 & 20\cos q_2 \\ \sin q_2 & 0 & \cos q_2 & 20\sin q_2 \\ 0 & -1 & 0 & 0 \\ 0 & 0 & 0 & 1 \end{bmatrix} \tag{42} $$

$$ {}^2\mathbf{T}_3 = \begin{bmatrix} \cos q_3 & -\sin q_3 & 0 & 10\cos q_3 \\ \sin q_3 & \cos q_3 & 0 & 10\sin q_3 \\ 0 & 0 & 1 & 10 \\ 0 & 0 & 0 & 1 \end{bmatrix} \tag{43} $$

where $q_1, q_2,$ and q_3 are the generalized variables representing joint displacements. Multiplying the matrices $\prod_{i=1}^{3} {}^{i}\mathbf{T}_{i-1}$, and extracting the (3×3) rotation matrix yields

$$ {}^{0}\mathbf{R}_{3} = \begin{bmatrix} \cos q_1 \cos q_2 \cos q_3 - \sin q_1 \sin q_3 & -\cos q_1 \cos q_2 \sin q_3 - \sin q_1 \cos q_3 & -\cos q_1 \sin q_2 \\ \sin q_1 \cos q_2 \cos q_3 + \cos q_1 \sin q_3 & -\sin q_1 \cos q_2 \sin q_3 + \cos q_1 \cos q_3 & -\sin q_1 \sin q_2 \\ \sin q_2 \cos q_3 & -\sin q_2 \sin q_3 & \cos q_2 \end{bmatrix} \quad (44) $$

The position vector is

$$ {}^{0}\mathbf{x}_{3} = \begin{bmatrix} 10\cos q_1 \cos q_2 \cos q_3 - 10\sin q_1 \sin q_3 - 10\cos q_1 \sin q_2 + 20\cos q_1 \cos q_2 \\ 10\sin q_1 \cos q_2 \cos q_3 + 10\cos q_1 \sin q_3 - 10\sin q_1 \sin q_2 + 20\sin q_1 \cos q_2 \\ 10\sin q_2 \cos q_3 + 10\cos q_2 + 20\sin q_2 + 50 \end{bmatrix} \quad (45) $$

6.1 Determining Singular Surfaces

For a general point $\mathbf{x} = \begin{bmatrix} x & y & z \end{bmatrix}^T$ on link 3 of the manipulator, the independent holonomic constraint equations are

$$ \Phi(\mathbf{q}) = \begin{bmatrix} x - 10\cos q_1 \cos q_2 \cos q_3 + 10\sin q_1 \sin q_3 + 10\cos q_1 \sin q_2 - 20\cos q_1 \cos q_2 \\ y - 10\sin q_1 \cos q_2 \cos q_3 - 10\cos q_1 \sin q_3 + 10\sin q_1 \sin q_2 - 20\sin q_1 \cos q_2 \\ z - 10\sin q_2 \cos q_3 - 10\cos q_2 - 20\sin q_2 - 50 \end{bmatrix} = \mathbf{0} \quad (46) $$

subject to the following joint limits

$$ -\frac{\pi}{4} \le q_1 \le \frac{5\pi}{4} \quad (47a) $$

$$ -\frac{\pi}{4} \le q_2 \le \frac{\pi}{2} \quad (47b) $$

$$ 0 \le q_3 \le 2\pi \quad (47c) $$

which are parametrized according to Eq. (6) as

$$ q_1 = b_1 + c_1 \sin\lambda_1 = \frac{\pi}{2} + \frac{3\pi}{4}\sin\lambda_1 \quad (48a) $$

$$ q_2 = b_2 + c_2 \sin\lambda_2 = \frac{\pi}{8} + \frac{3\pi}{8}\sin\lambda_2 \quad (48b) $$

$$ q_3 = b_3 + c_3 \sin\lambda_3 = \pi + \pi\sin\lambda_3 \quad (48c) $$

To evaluate the Jacobian with respect to the new generalized coordinates λ_i, the matrices $\mathbf{\Phi_q}$ and $\mathbf{q}_\lambda$ are evaluated such that

$$\mathbf{\Phi_q} = \begin{bmatrix} -10\sin q_1\cos q_2\cos q_3 - 10\cos q_1\sin q_3 + 10\sin q_1\sin q_2 - 20\sin q_1\cos q_2 \\ 10\cos q_1\cos q_2\cos q_3 - 10\sin q_1\sin q_3 - 10\cos q_1\sin q_2 + 20\cos q_1\cos q_2 \\ 0 \end{bmatrix}$$

$$\begin{matrix} -10\cos q_1\sin q_2\cos q_3 - 10\cos q_1\cos q_2 - 20\cos q_1\sin q_2 & -10\cos q_1\cos q_2\sin q_3 - 10\sin q_1\cos q_3 \\ -10\sin q_1\sin q_2\cos q_3 - 10\sin q_1\cos q_2 - 20\sin q_1\sin q_2 & -10\sin q_1\cos q_2\sin q_3 + 10\cos q_1\cos q_3 \\ 10\cos q_2\cos q_3 - 10\sin q_2 + 20\cos q_2 & -10\sin q_2\sin q_3 \end{matrix} \Bigg]$$

..... (49)

and

$$\mathbf{q}_\lambda = \begin{bmatrix} \frac{3\pi}{4}\cos\lambda_1 & 0 & 0 \\ 0 & \frac{3\pi}{8}\cos\lambda_2 & 0 \\ 0 & 0 & \pi\cos\lambda_3 \end{bmatrix} \tag{50}$$

Internal and boundary singularities are computed by evaluating the determinant of the Jacobian and equating to zero such that

$$\begin{aligned} \left|\mathbf{\Phi_q}\mathbf{q}_\lambda\right| &= 1125(-1)^{7/8}\cos\lambda_1\cos\lambda_2\cos\lambda_3\sin[\pi\sin\lambda_3] \\ &+(-4+2(-1)^{1/2})\left[(-1)^{1/4}+1\right]\cos\left(\frac{3\pi\sin\lambda_2}{8}\right)+(1+(-1)^{1/4})\cos\left(\frac{3\sin\lambda_2-8\sin\lambda_3}{8}\right) \\ &+(1+(-1)^{1/4})\cos\left(\frac{3\pi\sin\lambda_2}{8}+\pi\sin\lambda_3\right)+(2+4(-1)^{1/2})(1+(-1)^{1/4})\sin\left(\frac{3\pi\sin\lambda_2}{8}\right) \\ &-((-1)^{1/2}-(-1)^{3/4})\left[\sin\left(\frac{3\sin\lambda_2-8\sin\lambda_3}{8}\right)+\sin\left(\frac{3\pi\sin\lambda_2}{8}+\pi\sin\lambda_3\right)\right]=0 \end{aligned} \tag{51}$$

subject to the inequalities of Eq. (47). Singularities are determined by finding the roots of Eq. (51). For example, the term $\cos\lambda_1$ vanishes if $\lambda_1 = \pi/2$ or $\lambda_1 = -\pi/2$. Substituting λ_1 into Eq. (48a) results in $q_1 = -\frac{\pi}{4}$ or $q_1 = \frac{5\pi}{4}$. The other computed singularities are $q_3 = 0$, $q_3 = \pi$, $q_3 = 2\pi$, $q_2 = -\frac{\pi}{4}$, and $q_2 = \frac{\pi}{2}$. The total number of first-order singularities is seven. The singularity $q_3 = \pi$, however, is inside the interval [0 2π]. Since both of the endpoints are singularities, thus $q_3 = \pi$ will not be considered. Singular surfaces are parametrized by substituting each singularity into Eq. (45). Note, however, that some of these surfaces are boundary to the workspace, other surfaces are internal, and some surfaces have parts that are

on the boundary and parts that are internal. For example, substituting the singularity $q_1 = -\frac{\pi}{4}$ into Eq. (45) yields the singular surface parametrized as follows

$$\mathbf{x}^1(q_2, q_3) = \begin{bmatrix} 7.0711\cos q_2 \cos q_3 + 7.0711(\sin q_3 - \sin q_2) + 14.1421\cos q_2 \\ -7.0711\cos q_2 \cos q_3 + 7.0711(\sin q_3 + \sin q_2) - 14.1421\cos q_2 \\ 10\cos q_3 \sin q_2 + 10\cos q_2 + 20\sin q_2 + 50 \end{bmatrix} \tag{52}$$

with inequality constraints defined as

$$0 \le q_3 \le 2\pi \tag{53a}$$

$$-\pi/4 \le q_2 \le \pi/2 \tag{53b}$$

Singular surface $\mathbf{x}^1(q_2, q_3)$ is shown in Fig. (10a).

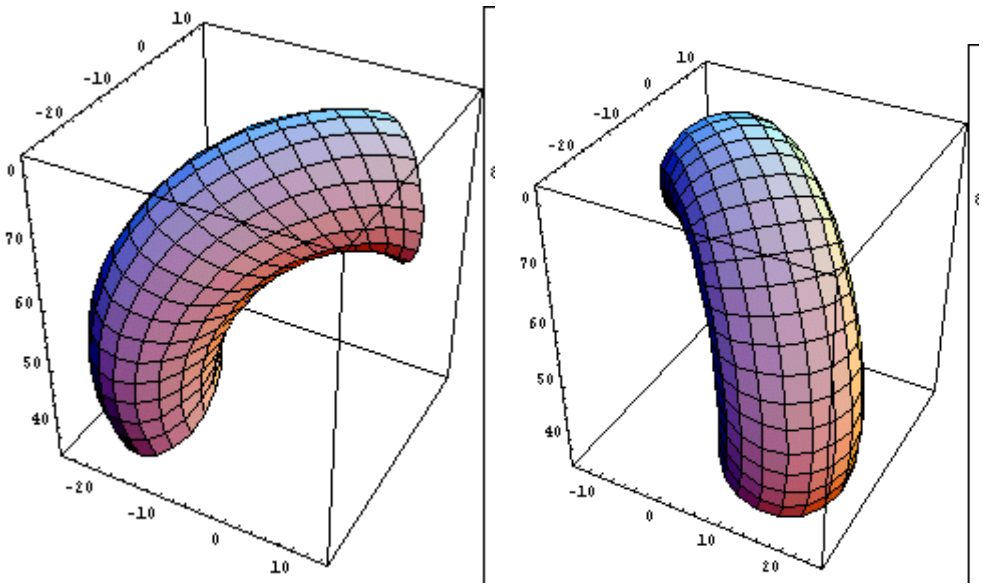

Fig. 10 (a) Singular surfaces (a) $\mathbf{x}^1(q_2, q_3)$ due to $q_1 = -\pi/4$, (b) $\mathbf{x}^2(q_2, q_3)$ due to $q_1 = 5\pi/4$

Substituting the singularity $q_1 = \frac{5\pi}{4}$ into Eq. (45) yields the singular surface

$$\mathbf{x}^2(q_2, q_3) = \begin{bmatrix} -7.0711\cos q_3 \cos q_2 + 7.0711(\sin q_3 + \sin q_2) - 14.1421\cos q_2 \\ -7.0711\cos q_3 \cos q_2 - 7.0711(\sin q_3 - \sin q_2) - 14.1421\cos q_2 \\ 10\cos q_3 \sin q_2 + 10\cos q_2 + 20\sin q_2 + 50 \end{bmatrix} \tag{54}$$

with inequality constraints as

$$0 \le q_3 \le 2\pi \tag{55a}$$

$$-\pi/4 \le q_2 \le \pi/2 \tag{55b}$$

The singular surface $\mathbf{x}^2(q_2, q_3)$ is shown in Fig. (10b).

Singular surfaces due to the singularities $q_3 = 0$, $q_3 = 2\pi$, $q_2 = -\frac{\pi}{4}$, and $q_2 = \frac{\pi}{2}$ are depicted in Fig. (11) a, b, c, and d, respectively.

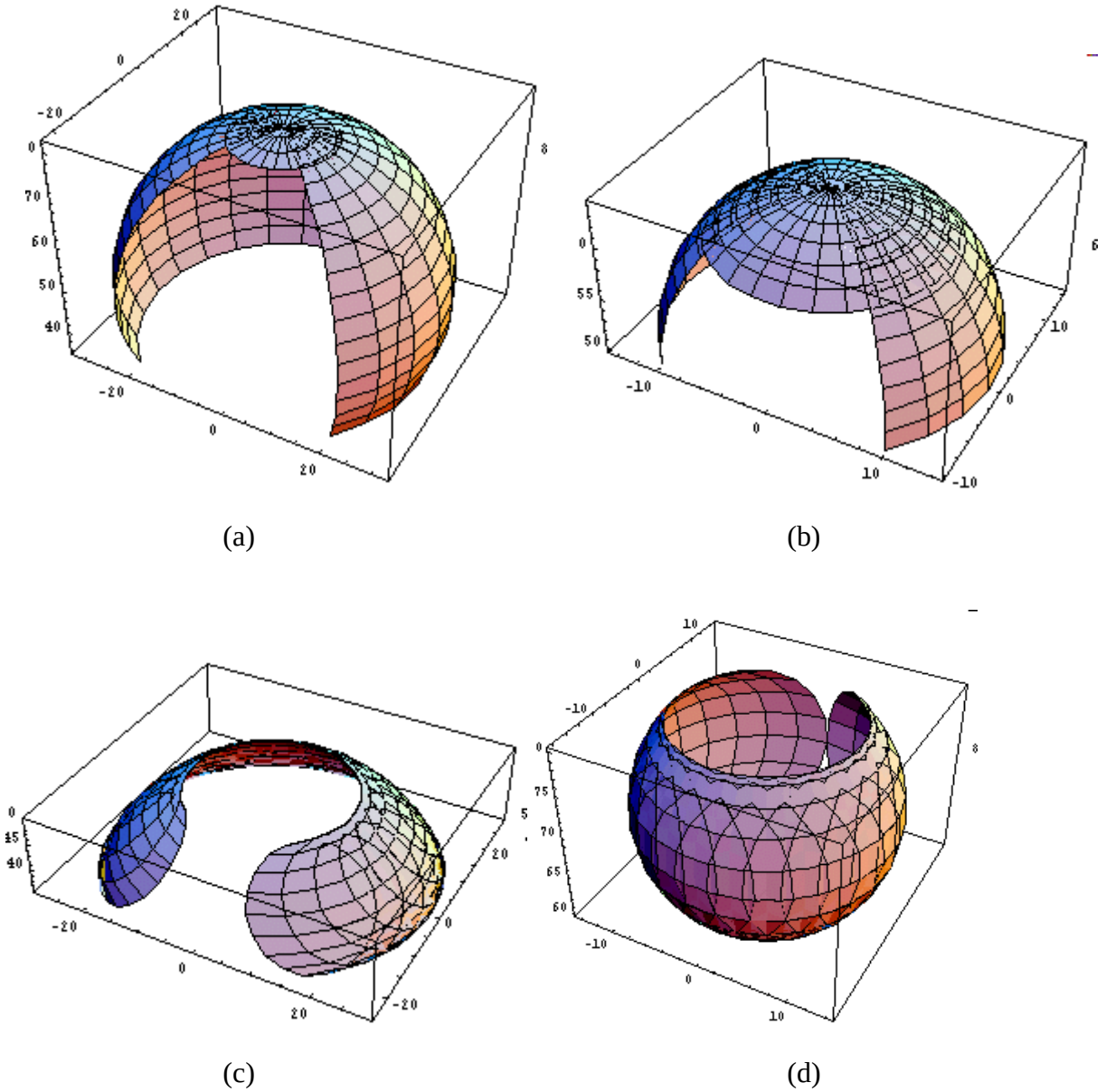

(a) (b)

(c) (d)

Fig. 11 Singular surfaces due to first order singularities

6.2 Determining Subsurfaces

Singular surfaces are divided into subsurfaces by computing curves of intersection between them. Once these curves are determined and projected onto their respective parametric space of two variables, each region representing a subsurface is studied for existence on the boundary of the workspace. To illustrate the determination of subsurfaces, consider the intersection of the two surfaces $\mathbf{x}^1(q_2, q_3)$ and $\mathbf{x}^2(q_2, q_3)$. The parameters of the second surface will be changed to t_1 and t_2 such that $t_1 = q_2$ and $t_2 = q_3$. The marching method presented in section 3.2 is implemented. The constraint matrix (Eq. 10) can be written as

$$\mathbf{H}(\mathbf{q}) = \begin{bmatrix} \mathbf{x}^1(q_2, q_3) - \mathbf{x}^2(t_1, t_2) \\ q_2 - \frac{\pi}{2} - \frac{3\pi}{4}\sin\lambda_1 \\ q_3 - \frac{\pi}{8} - \frac{3\pi}{8}\sin\lambda_2 \\ t_1 - \frac{\pi}{2} - \frac{3\pi}{4}\sin\lambda_3 \\ t_2 - \frac{\pi}{8} - \frac{3\pi}{8}\sin\lambda_4 \end{bmatrix} = \mathbf{0} \tag{56}$$

The starting point $\mathbf{s}^*$ computed using the Moore-Penrose pseudo inverse is $\mathbf{s}^* = [0.6184 \quad 3.4086 \quad 0.6184 \quad 2.8745 \quad 0.1928 \quad 0.0851 \quad 0.1928 \quad -.0851]$. Using $\mathbf{s}^*$ as a starting point, the algorithm for mapping marching curves is employed to continue tracing the curves. In this special case, a bifurcation point is encountered at $\mathbf{s}^o = [0.7854 \quad 3.1416 \quad 0.7854 \quad 3.1416 \quad 0.3398 \quad 0.8306\times10^{-9} \quad 0.3398 \quad -0.8306\times10^{-9}]$. Two tangents are required to continue tracing. The computed intersection curves in the parametric space are depicted in Fig. (12a), and depicted on the surfaces in Fig. (12b).

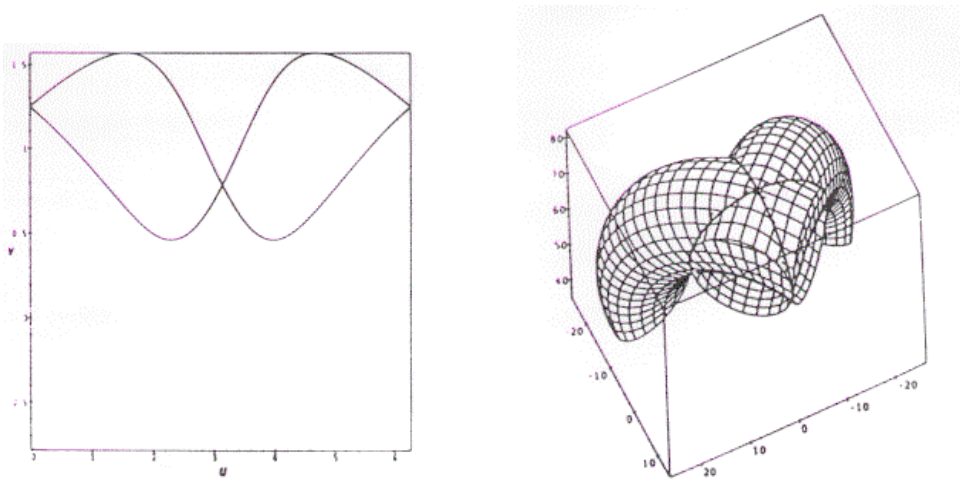

(a) (b)

Fig. 12 Intersection Curves Between $\mathbf{x}^1$ and $\mathbf{x}^2$ (a) in the uv-space, (b) on the surfaces

In addition to the intersection curves resulting from the intersection between $\mathbf{x}^1(q_2, q_3)$ and $\mathbf{x}^2(q_2, q_3)$, surface $\mathbf{x}^1(q_2, q_3)$ intersects with other singular surfaces. The computed intersection curves due to other singular surfaces are superpositioned in Fig. 13. These four singular curves ($\mathbf{c}^1$, $\mathbf{c}^2$, $\mathbf{c}^3$ and $\mathbf{c}^4$) partition surface $\mathbf{x}^1$ into twelve subsurfaces.

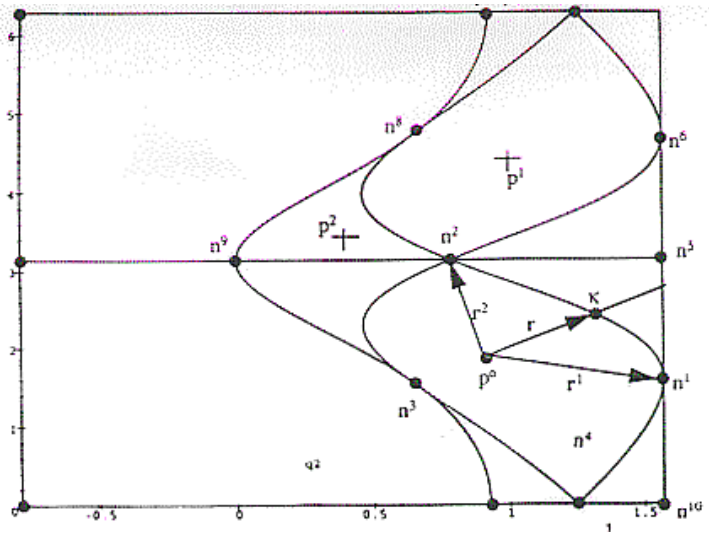

Fig. 13 Intersection curves dividing singular surface $\mathbf{x}^1$ into subsurfaces

It is necessary to determine the intersection of these curves in order to define the boundary of each subsurface. Singular curves shown in Fig. 13 are computed numerically, thus, it is

difficult to parametrize these curves. The grid method is thus used to determine points of intersection.

To determine whether each subsurface is a boundary or internal subsurface to the wrist workspace, the perturbation method (Eq. 44) is implemented. For example, consider the point $p^1(\mathbf{q})$ on the subsurface Ψ^1 which has the set of generalized coordinates $q_2 = 0.4$ and $q_3 = 3.4$. Note that the subsurface Ψ^1 is defined as follows

$$\Psi^1 = \begin{bmatrix} 7.0711\cos q_2 \cos q_3 + 7.0711(\sin q_3 - \sin q_2) + 14.1421\cos q_2 \\ -7.0711\cos q_2 \cos q_3 + 7.0711(\sin q_3 + \sin q_3) - 14.1421\cos q_2 \\ 10\cos q_2 \sin q_3 + 10\cos q_2 + 20\sin q_2 + 50 \end{bmatrix} \tag{57}$$

enclosed by the following boundary curve segments: c^1 on the interval $\left[n^2 \; n^8\right]$, c^3 on the interval $\left[n^8 \; n^9\right]$, and c^4 on the interval $\left[n^9 \; n^2\right]$. To determine the normal to Ψ^1 using Eq. (43), partial derivatives representing tangent vectors are evaluated such that

$$\frac{\partial \psi^1}{\partial q_2} = \begin{bmatrix} -7.07\sin q_2 \cos q_3 - 7.07\cos q_2 - 14.14\sin q_2 \\ 7.07\sin q_2 \cos q_3 + 7.07\cos q_2 + 14.14\sin q_2 \\ 10\cos q_2 \cos q_3 - 10\sin q_2 + 20\cos q_2 \end{bmatrix} \tag{58}$$

and

$$\frac{\partial \psi^1}{\partial q_3} = \begin{bmatrix} -7.07\cos q_2 \sin q_3 + 7.07\cos q_3 \\ 7.07\cos q_2 \sin q_3 + 7.07\cos q_3 \\ -10\sin q_2 \sin q_3 \end{bmatrix} \tag{59}$$

The normal is computed

$$\mathbf{n} = \frac{\partial \psi^1}{\partial q_2} \times \frac{\partial \psi^1}{\partial q_3} =$$

$$= \begin{bmatrix} \frac{707}{-10}\left(\cos q_2 (\cos q_3)^2 - \sin q_3 \cos q_3 - \sin q_3 + \sin q_2 \cos q_3 - 2\cos q_2 \cos q_3\right) \\ \frac{707}{-10}\left(\cos q_3 \sin q_2 + \cos q_2 (\cos q_3)^2 - 2\sin q_3 - \cos q_3 \sin q_3 + \cos q_2 \cos q_3\right) \\ \frac{499849}{-5000}\left(\sin q_2 \cos q_3 - \cos q_2 \cos q_3 - \sin q_2 (\cos q_3)^2\right) \end{bmatrix} \tag{60}$$

The unit normal $\hat{\mathbf{n}} = \mathbf{n}/\|\mathbf{n}\|$ at the point $\mathbf{q}^o$ on the subsurface Ψ^1 is evaluated

$$\hat{\mathbf{n}} = \mathbf{n}/\|\mathbf{n}\| = \begin{bmatrix} 0.098 & -0.452 & 0.887 \end{bmatrix}^T \tag{61}$$

For a small perturbation $\partial\varepsilon = +0.1$, the coordinates of the perturbed point are computed as

$$\mathbf{x}_1 = \Psi^i(\mathbf{q}^o) + \partial\varepsilon\hat{\mathbf{n}}(\mathbf{q}^o) = \begin{bmatrix} 6.513 & -1.812 & 63.418 \end{bmatrix}^T \tag{62}$$

Forming Eq. (19) with $\mathbf{x}_1$ and the inequalities of Eq. (47), there exists a solution such the generalized set is $\mathbf{q} = \begin{bmatrix} 2.321 & 1.222 & -3.502 \end{bmatrix}^T$. For a perturbation of $\partial\varepsilon = -0.1$, the coordinates of the perturbed point are

$$\mathbf{x}_2 = \Psi^i(\mathbf{q}^o) - \partial\varepsilon\hat{\mathbf{n}}(\mathbf{q}^o) = \begin{bmatrix} 6.494 & -1.721 & 63.241 \end{bmatrix}^T \tag{63}$$

and the solution for this position is the generalized set $\mathbf{q} = \begin{bmatrix} 2.393 & 1.231 & -3.463 \end{bmatrix}^T$. Thus, both perturbation points are inside the wrist workspace which guarantees that this subsurface is an internal one. For subsurface Ψ^2, the point on this subsurface is chosen as $p^2(\mathbf{q})$ which has coordinates $q_2 = 1.0$ and $q_3 = 4.4$. The unit normal $\hat{\mathbf{n}} = \mathbf{n}/\|\mathbf{n}\|$ at this point on the subsurface Ψ^2 is evaluated as

$$\hat{\mathbf{n}} = \mathbf{n}/\|\mathbf{n}\| = \begin{bmatrix} 0.671 & 0.653 & 0.351 \end{bmatrix}^T \tag{64}$$

For a small perturbation $\partial\varepsilon = +0.1$, the coordinates of the perturbed point are

$$\mathbf{x}_1 = \Psi^i(\mathbf{q}^o) + \partial\varepsilon\hat{\mathbf{n}}(\mathbf{q}^o) = \begin{bmatrix} -6.211 & -7.245 & 69.646 \end{bmatrix}^T \tag{65}$$

For this perturbed point, a solution of Eq. (19) subject to inequality constraints of Eq. (47) can be found such that the set of generalized coordinates is $\mathbf{q} = \begin{bmatrix} 2.276 & 1.114 & 1.882 \end{bmatrix}^T$. A solution, however, *cannot be found* for $-\partial\varepsilon$. This indicates that Ψ^2 is a boundary subsurface to the wrist workspace. Using this technique, boundary subsurfaces of each singular surface are determined. These surfaces are depicted in Fig. 14. The volume enclosed by these surfaces is the wrist workspace.

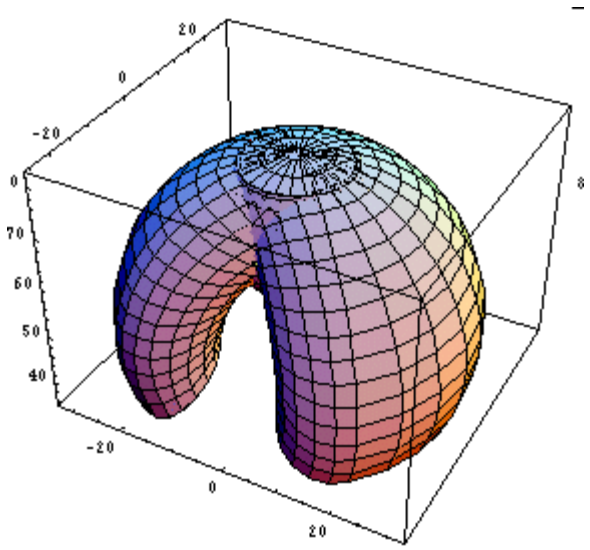

Fig. 14 Analytical surfaces that are boundary to the workspace

6.3 Developing Atlases of Orientability

An atlas of orientability will be developed for the manipulator studied in the previous section at a point in the workspace located at $\mathbf{p} = \begin{bmatrix} 0 & -25 & 55 \end{bmatrix}^T$. Analytical boundary to the wrist workspace was developed and is shown in Fig. 14 . A service sphere is located at **p** as shown in Fig. (15a). The surface of the sphere is intersected with the boundary to the workspace. Intersection curves are depicted in Fig. 15b.

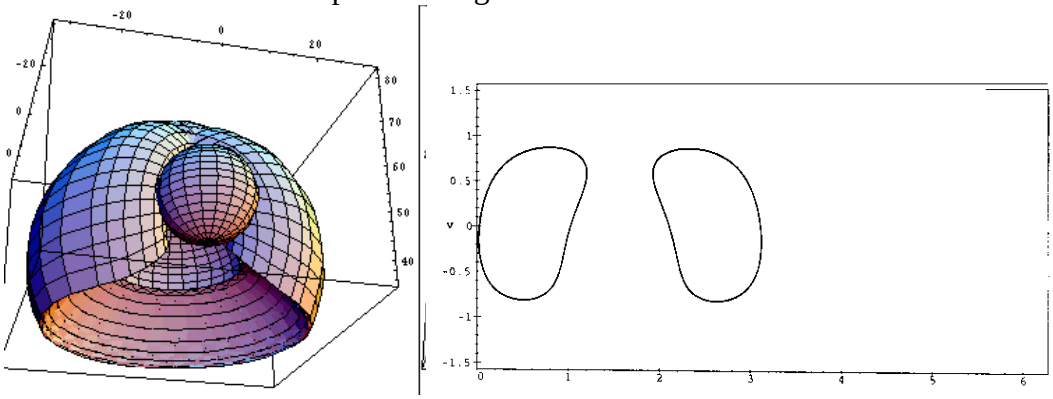

Fig. 15 (a) $\mathbf{x}_{ss}(u,v)$ at an operating point (b) Service regions due to the wrist workspace

7. Service Regions due to Distal joints

For a point $\mathbf{p} = \begin{bmatrix} -11.53 & 15.281 & 75.605 \end{bmatrix}^T$ in the reachable workspace, it is necessary to determine service regions due to constraints of the distal joints. For the manipulator discussed in this example, the distal joints have the following constraints.

$$-110^o \le q_4 \le 110^o \tag{66a}$$

$$-120^o \le q_5 \le 120^o \tag{66b}$$

$$-30^o \le q_6 \le 240^o \tag{66c}$$

For a point described as the vector ${}^6\mathbf{x}_E = \begin{bmatrix} 0 & 0 & 2 \end{bmatrix}^T$ resolved in the sixth frame and substituting for $q_4, q_5,$ and q_6 into Eq. (26) results in a system of three equations with three unknowns. The coordinates of the wrist point are calculated and presented in Table (1).

Table (1) Calculated joint coordinates and wrist point coordinates

	$q_4, q_5,$ and q_6	calculated $q_1, q_2,$ and q_3	calculated wrist point
1.	$q_4 = 110^o, q_5 = 120^o,$ $q_6 = -30^o$	$q_1 = 53.98^o, q_2 = 89.807^o,$ $q_3 = -122.554^o$	$\mathbf{w}_1 = \begin{bmatrix} 11.176 & -20.462 & 56.581 \end{bmatrix}^T$
2.	$q_4 = 110^o, q_5 = 120^o,$ $q_6 = 240^o$	$q_1 = -53.104^o, q_2 = -51.124^o,$ $q_3 = -111.635^o$	$\mathbf{w}_2 = \begin{bmatrix} -9.848 & -25.59 & 47.882 \end{bmatrix}^T$
3.	$q_4 = 110^o, q_5 = -120^o$ $, q_6 = -30^o$	$q_1 = 134.698^o, q_2 = 162.093^o$ $q_3 = 87.502^o$	$\mathbf{w}_3 = \begin{bmatrix} -1.476 & -34.018 & 46.969 \end{bmatrix}^T$
4.	$q_4 = 110^o, q_5 = -120^o$ $, q_6 = 240^o$	$q_1 = -141.712^o, q_2 = 20.805^o$ $q_3 = 94.773^o$	$\mathbf{w}_4 = \begin{bmatrix} 5.076 & -27.733 & 65.713 \end{bmatrix}^T$
5.	$q_4 = -110^o, q_5 = 120^o,$ $q_6 = -30^o$	$q_1 = 36.048^o, q_2 = 164.627^o,$ $q_3 = -94.44^o$	$\mathbf{w}_5 = \begin{bmatrix} -1.559 & -31.962 & 45.147 \end{bmatrix}^T$

Table (1) continued

	$q_4, q_5,$ and q_6	calculated $q_1, q_2,$ and q_3	calculated wrist point
6.	$q_4 = -110^o, q_5 = 120^o,$ $q_6 = 240^o$	$q_1 = -43.603^o, q_2 = 15.815^o,$ $q_3 = -90.925^o$	$\mathbf{w}_6 = [-5.56 \quad -29.225 \quad 64.962]^T$
7.	$q_4 = -110^o, q_5 = -120^o$ $, q_6 = -30^o$	$q_1 = -125.767^o, \ q_2 = -49.123^o$ $q_3 = 112.224^o$	$\mathbf{w}_7 = [10.325 \quad -25.261 \quad 48.572]^T$
8.	$q_4 = -110^o, q_5 = -120^o$ $, q_6 = 240^o$	$q_1 = 232.854^o, q_2 = -58.873^o$ $q_3 = 117.719^o$	$\mathbf{w}_8 = [9.858 \quad -23.637 \quad 48.003]^T$

Wrist points are located on the service sphere and the uv-parameters are calculated for each point such that

$$\begin{bmatrix} w_x \\ w_y \\ w_z \end{bmatrix} - \begin{bmatrix} p_x + h\cos v\cos u \\ p_y + h\cos v\sin u \\ p_z + h\sin v \end{bmatrix} = \mathbf{0} \tag{67}$$

Curves joining wrist points are calculated using Eq. (28) and depicted in Fig. (16)

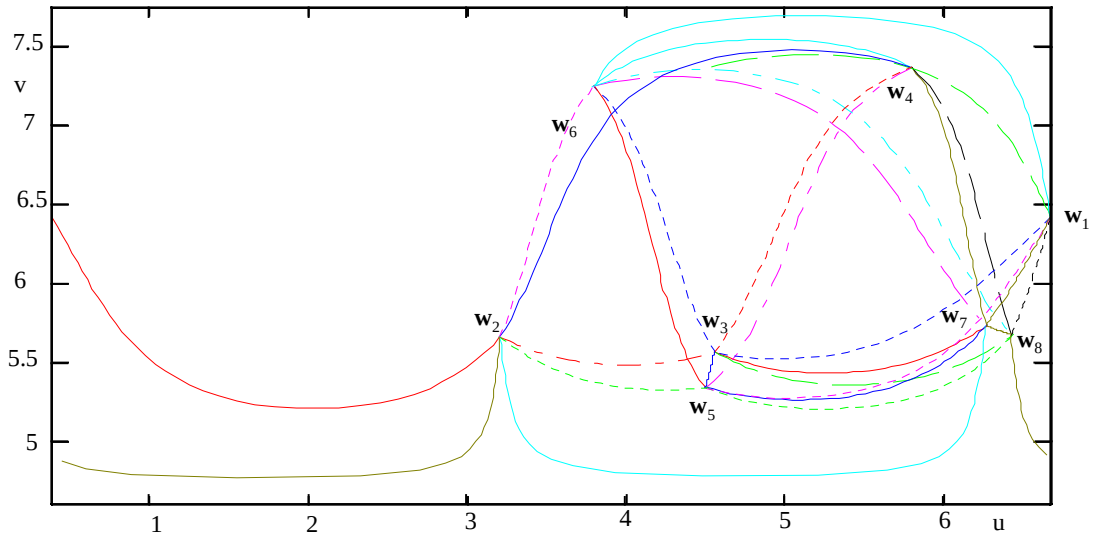

Fig. 16 Curves joining Wrist Points

The regions inside the resulting curves can be determined to be no-service regions. The atlas of orientability at the point **p** is the superposition of all service regions (Fig. 15b and Fig. 16.) .

8. Optimization of the Location of the Manipulator

Using the wrist workspace concept, it is possible to develop criteria for choosing a suitable location for the manipulator to achieve maximum orientability. Since the wrist workspace has been analytically formulated, it is now possible to locate the service sphere such that it is entirely inside the boundary of the wrist workspace. This guarantees that any potential wrist location will be attained. This is illustrated in the following example. Consider the six degree-of-freedom manipulator depicted in Fig. (17a). The wrist workspace is formulated using the methods developed earlier and is shown in Fig. (17b).

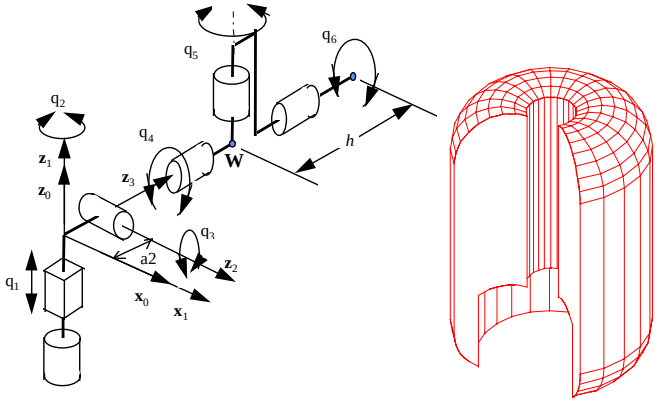

Fig. 17 (a) A six degree-of-freedom manipulator (b) Wrist workspace

Consider the orientability of this manipulator at a target in the workspace. By changing the location of the manipulator with respect to the service sphere such that the sphere is completely inside the wrist workspace, the orientability of the manipulator at this point is increased. Figure (18a) depicts a location of a manipulator with respect to a target. This position corresponds to having the service sphere located partly outside the wrist workspace as depicted in Fig. (18b).

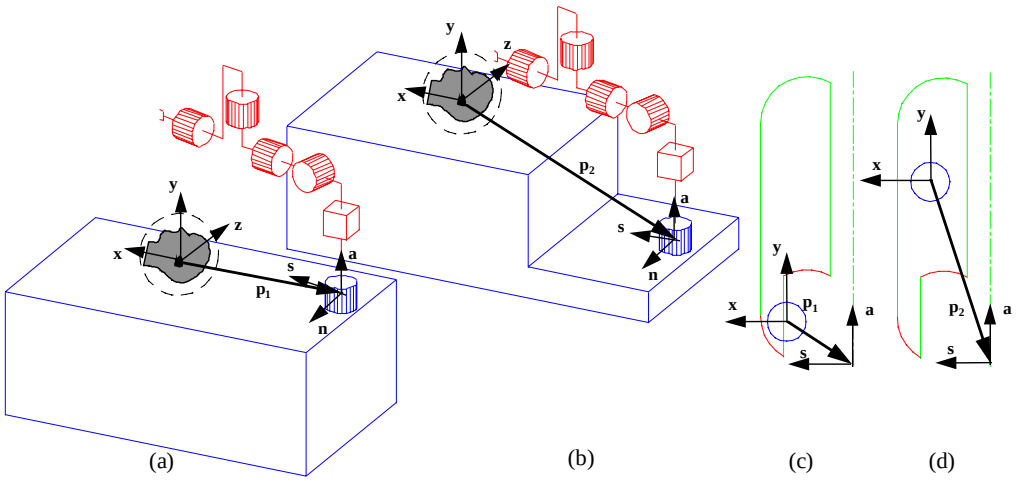

Fig. 18 Locating the service sphere with respect to a manipulator (a) position 1 (b) position 2 (c) A cross section of the workspace depicting the location of the service sphere and (d) the location of the service sphere for maximum dexterity

9 Conclusions

Analytical formulation for determining atlases of orientability at a point in the workspace were presented. The method is applicable for a general class of manipulators. It has been shown that atlases of orientability are applicable to robot-assisted surgery where a surgeon can obtain a better understanding of possible orientations of the surgical tool. Criteria for determining a location for the manipulator can be chosen using this method such that maximum orientability can be obtained.

It has been shown that singular surfaces can be partitioned into subsurfaces. The boundary of these subsurfaces are defined by determining singular curves that result from the intersection of two singular surfaces. It has been shown that subsurfaces can be entirely on the boundary of the workspace or entirely inside the workspace. Difficulties in computing second-order singularities were encountered when similar parametric surfaces intersect. Since singular curves are computed numerically using marching methods, difficulties in parameterizing these curves occurred.

It is noted that because analytical representations of the boundary to the workspace were obtained, it was possible to determine intersections of the service sphere with the parametric surface patches. Other methods have succeeded in presenting only numerical results. It is also noted that the use of the Moore-Penrose pseudo inverse method in determining the intersection curves for singular surfaces, has facilitated the automation of the method with adequate accuracy. The authors are in the process of developing a method to parameterize singular curves as well as to automatically select a point on the subsurface by computing its centroid.

Acknowledgements

This work was funded in part by a research initiation award from the Society of Manufacturing Engineers (SME), and a NATO Collaborative Linkage grant.

References

[1] P. A. Finlay, "The Development of Advanced Medical Robots," Proceedings of the 21st International Symposium on Industrial Robots, Copenhagen, Germany, *IFS Publications*, 1990, pp. 209-214.

[2] Y.S. Kwoh, "A Robot with Improved Absolute Positioning Accuracy for CT Guided Stereotactic Brain Surgery," IEEE Transactions on Biomedical Engineering, Vol. 35, No. 2, 1988, pp. 153-160.

[3] A. L. Benabid, et al., "Computer-Driven Robot for Stereotactic Surgery Connected to CT Scan and Magnetic Resonance Imaging: Technological Design and Preliminary Results." Applied Neurophysiology, Vol. 50, Nos. 1-6, 1987, pp. 153-154.

[4] S. Lavallee, and P. Cinquin, "IGOR: Image Guided Operating Robot," ICAR, 1991, pp. 876-881.

[5] Kumar, A. and Waldron, K. J. 1981. The workspaces of a mechanical manipulator. *ASME J. of Mech. Des.*, 103(3):665-672.

[6] Tsai, Y.C. and Soni, A.H. 1981, "Accessible Region and Synthesis of Robot Arm," *ASME J. of Mech. Design*, Vol. 103, pp. 803-811.

[7] Gupta, K.G. and Roth, B. 1982, "Design Considerations for Manipulator Workspace," ASME *Journal of Mechanical Design*, Vol. 104, No. 4, pp. 704-711.

[8] Haug, E.J., Adkins, R., and Luh, C.M., 1994, "Numerical Algorithms for Mapping Boundaries of Manipulator Workspaces," *Proceedings of the 23rd ASME Mechanisms Conference*, Minneapolis, MN.

[9] Qiu, C.C., Luh, C.M., and Haug, E.J. 1995. Dexterous workspaces of manipulators, Part III: calculation of continuation curves at bifurcation points. To appear in *ASME J. of Mechanical Design*.

[10] Ceccarelli, M. and Vinciguerra, A., 1995, "On the Workspace of General 4R Manipulators," *International Journal of Robotics Research*, Vol. 14, No. 2, pp. 152-160

[11] Yang, D.C.H. and Lee, T.W. 1983. On the workspace of mechanical manipulators. *J. of Mechanisms, Transmission and Automation Design*, Vol. 105, pp. 62-69.
[12] Yang, D.C.H. and Lai, Z.C. On the dexterity of robotic manipulators-service angle. *Transactions of ASME, J.of Mech., Transm., and Automation in Design*, Vol. 107.
[13] Lai, Z.C. and Menq., C. 1988. The dexterous workspace of simple manipulators. *IEEE J. Robotics and Automation*, Vol. 4, No. 1.
[14] Wang, J.Y. and Wu, J.K. 1993. Dexterous workspaces of manipulators, part 2: computational methods. *Mechanics of Structures and Machines*, Vol. 21, No. 4, pp. 471-506.
[15] Emiris, D.M. 1993. Workspace analysis of realistic elbow and dual-elbow robot. *Mechanisms and Machine Theory*, Vol. 28, No. 3, pp. 375-396.
[16] Agrawal, S.K. 1990. Workspace boundaries of in-parallel manipulator systems. *Int. J. of Robotics and Automation*, Vol. 7, No. 2, pp. 94-99.
[17] Gosselin, C. and Angeles, J. 1990. Singularity analysis of closed loop kinematic chains. *IEEE Trans. on Robotics and Automation*, Vol. 6, No. 3, pp. 281-290.
[18] Pennock, G.R. and Kassner, D.J. 1993. The workspace of a general planar three-degree-of-freedom platform-type manipulator. *Journal of Mechanical Design*, Vol. 115, pp. 269-276.
[19] Sugimoto, K. Duffy, J. andHunt, K. H. 1982. Special configurations of spatial mechanisms and robot arms. *Mechanism and Machine Theory*, 117(2):119-132.
[20] Wang, S. L. and Waldron, K. J. 1987. Study of the singular configurations of serial manipulators. *ASME J. of Mech., Trans., and Autom. in Des*., **109**(1):14-20.
[21] Waldron, K. J. Wang, S. L. and Bolin, S. L. 1985. A study of the Jacobian matrix of serial manipulators. *ASME J. of Mech., Trans., and Autom. in Des*., **107**(2):230-238.
[22] Shu, M. Kohli, D. and Dwivedi, S. H. 1986. *Proceedings of the 6th World Congress on Theory of Machines and Mechanisms*, New Delhi, India, 988-993.
[23] Litvin, F. L. Fanghella, P. Tan, J. and Zhang, Y. 1986. Singularities in motion and dispplacement functions of spppatial linkages. *ASME J. of Mech., Trans., and Autom. in Des.*, **108**(4):516-523.
[24] Litvin, F. L. Yi, Z. Castelli, V. P. and Innocenti, C. 1986. Singularities, configurations, and displacement functions for manipulators. *Int. J. Rob. Res.*, **5**(2):52-65.
[25] Lipkin, H. and Pohl, E. 1991. Enumeration of singular configurations for robotic manipulators. *ASME J. Mech., Trans., and Autom. in Des*., **113:**272-279
[26] Shamir, T. 1990. The singularities of redundant robot arms. *Int. J. of Rob. Res.*, **2**(1):113-121.
[27] Gorla, B. 1981. Influence of the control on the structure of a manipulator from a kinematic point of view. *Proc. 4th Symp. Thoery and Practice of Rob. Manipulators*, Zaborow, Poland, 30-46.
[28] Soylu, R. and Duffy, J. 1988. Hypersurfaces of special configurations of serial manipulators and related concepts. Part II: Passive joints, configurations, component manifolds and some applications. *J. Rob. Systems*, **5**:31-53.
[30] Waldron, K. J. 1987. Operating barriers within the workspace of manipulators. *Proceedings of the Society of Manufacturing Engineers, Chicago, IL, Robots II/17th ISIR*, **8:**35-46.
[29] Lai, Z. C. and Yang, D. C. H. 1984. On the singularity analysis of simple six-link manipulators ASME Paper No. 84-DET-220.
[31] Nielsen, L. deWitt, C. C. and Hagander, P. 1991. Controllability issues of robots in singular configurations. *Proceedings of IEEE Int. Conf. on Rob. and Autom.*, Sacramento, CA.
[32] K. Abdel-Malek and H.J. Yeh, "Analytical Boundary of the Workspace for General Three Degree-of-Freedom Mechanisms," (in press) *International Journal of Robotics Research.*
[33] G. Lucaks, "Simple Singularities in Surface-surface Intersections," *The Mathematics of Surfaces*, (ed. Gregory, J.A.), Clarendon Press, Oxford, 1990.
[34] J. Denavit and R.S. Hartenberg, "A kinematic notation for lower-pair mechanisms based on matrices. *Journal of Applied Mechanics, ASME*, Vol. 22, 1955, pp. 215-221.

[35] E.L. Allgower and K. Georg, *Numerical Continuation Methods: An Introduction*, Springer-Verlag, Berlin, 1990.
[36] G. Muellenheim, "On Determining Start Points for a Surface/surface Intersection Algorithm," *Computer Aided Geometric Design* Vol. 8, No. 5, 1991, pp. 401-408.
[37] M.J. Pratt, and A.D. Geisow, "Surface/surface Intersection Problems," *The Mathematics of Surfaces*, (ed. Gregory, J.A.), Clarendon Press, Oxford, 1986.
[38] H. B. Keller, *Lectures on Numerical Methods in Bifurcation Problems*. Springer Verlag, Berlin, Heidelberg, New York, 1987.
[39] W.C. Rheinboldt, *Numerical Analysis of Parametrized Nonlinear Equations*, John Wiley and Sons, New York, 1986.
[40] D. Glauser, P. Flury, and C.W. Burckhardt, "Mechanical Concept of the Neurosurgical Robot 'Minerva'," Robotica, Vol. 11, 1993, pp. 567-575.